Nat. Hazards Earth Syst. Sci., 18, 869–887, 2018
https://doi.org/10.5194/nhess-18-869-2018

Natural Hazards and Earth System Sciences
Open Access
EGU

Modeling the influence of snow cover temperature and water content on wet-snow avalanche runout

Cesar Vera Valero[1], **Nander Wever**[2], **Marc Christen**[1], **and Perry Bartelt**[1]

[1]WSL Institute for Snow and Avalanche Research SLF, Flüelastrasse 11, 7260 Davos Dorf, Switzerland
[2]École Polytechnique Fédérale de Lausanne (EPFL), School of Architecture, Civil and Environmental Engineering, Lausanne, Switzerland

Correspondence: Cesar Vera Valero (cesar.vera@slf.ch)

Received: 25 January 2017 – Discussion started: 7 March 2017
Revised: 3 February 2018 – Accepted: 8 February 2018 – Published: 19 March 2018

Abstract. Snow avalanche motion is strongly dependent on the temperature and water content of the snow cover. In this paper we use a snow cover model, driven by measured meteorological data, to set the initial and boundary conditions for wet-snow avalanche calculations. The snow cover model provides estimates of snow height, density, temperature and liquid water content. This information is used to prescribe fracture heights and erosion heights for an avalanche dynamics model. We compare simulated runout distances with observed avalanche deposition fields using a contingency table analysis. Our analysis of the simulations reveals a large variability in predicted runout for tracks with flat terraces and gradual slope transitions to the runout zone. Reliable estimates of avalanche mass (height and density) in the release and erosion zones are identified to be more important than an exact specification of temperature and water content. For wet-snow avalanches, this implies that the layers where meltwater accumulates in the release zone must be identified accurately as this defines the height of the fracture slab and therefore the release mass. Advanced thermomechanical models appear to be better suited to simulate wet-snow avalanche inundation areas than existing guideline procedures if and only if accurate snow cover information is available.

1 Introduction

Avalanche hazard mitigation has historically concentrated on catastrophic avalanches releasing from dry, high alpine snow covers. There are many regions in the world, however, where wet-snow avalanche problems are dominant. Increasingly, avalanche engineers require methods to consider the avalanche hazard arising from frequent wet-snow slides (Naaim et al., 2013).

The runout of wet-snow avalanches is especially difficult to calculate because temperature and liquid water content (LWC) have a strong influence on the mechanical properties of snow (Denoth, 1982; Voytokskiy, 1977; Salm, 1982). When warm snow contains liquid water, the deformation mechanics are controlled by the liquid film at the grain-to-grain contact (Salm, 1982). Wet snow can be plastically deformed until it reaches "packed density". Granules in wet-snow avalanches are therefore large, heavy and poorly sorted in comparison to granules in dry avalanches (Jomelli and Bertran, 2001; Bartelt and McArdell, 2009). The bulk flow viscosity and cohesion of wet-snow avalanches is larger than in dry flows (Bartelt et al., 2015). The formation of levees with steep vertical shear planes in wet-snow avalanche deposits is another indication of the viscous and cohesive character of wet-snow avalanches (Bartelt et al., 2012b).

An increased bulk flow viscosity, however, is not the only mechanical change induced by warm, moist snow. The presence of liquid water on interacting snow surfaces *decreases* the magnitude of the *bulk* sliding friction coefficient. This decrease has been observed and quantified in many experiments, particularly those involving ski friction (Glenne, 1987; Colbeck, 1992). The decrease in sliding friction results in long-runout avalanches Naaim et al. (2013), making wet-snow flows particularly dangerous.

To model the lower flow velocities associated with wet-snow flows, the Swiss guidelines on avalanche calculation

recommend increasing the velocity-squared turbulent friction (Salm et al., 1990). Wet-snow avalanches are therefore treated as dense granular flows in the frictional flow regime (Voellmy, 1955; Bozhinskiy and Losev, 1998). Because measured velocity profiles of wet-snow avalanches exhibit pronounced viscoplastic, plug-like character, they are often modeled with a Bingham-type flow rheology (Dent and Lang, 1983; Norem et al., 1987; Salm, 1993; Dent et al., 1998; Bartelt et al., 2005; Kern et al., 2009). Bartelt et al. (2015) uses cohesion to reduce the random kinetic energy of the avalanche core which effectively hinders avalanche fluidization and prevents the formation of mixed flowing/powder avalanches (Buser and Bartelt, 2015).

The sensitivity of wet-snow avalanche flow on temperature and moisture content makes predictions of avalanche runout difficult. For example, wet-snow avalanches often occur after extreme precipitation events followed by intense warming. Because of differences in snow cover temperature and water content between the release and runout zones, wet-snow avalanches can start in sub-zero temperatures and run into moist, isothermal snow covers. That is, sub-zero release areas can lead to the formation of dry mixed flowing/powder type avalanches that transition at lower elevations to moist, wet flows. Clearly, a wet-snow avalanche model must account for the initial temperature and water content of the snow cover.

In this paper we use snow cover models to establish the initial and boundary conditions for wet-snow avalanche dynamics calculations. We specify snow cover information that is derived from detailed physics-based snow cover model simulations using SNOWPACK (Bartelt and Lehning, 2002; Lehning et al., 2002). Unlike existing approaches (e.g., Gruber and Bartelt, 2007), avalanche dynamics parameters will not be tuned but are fixed within the framework of empirical functions parameterized by snow density, temperature and moisture content (Vera Valero et al., 2015, 2016). Our goal is to obtain accurate runout and deposition predictions without ad hoc modifications to avalanche model parameters. Instead of parameter optimization, we specify snow height, density, temperature and moisture content in both release (initial conditions) and entrainment zones (boundary conditions) as input data for the model.

The approach consists of three basic steps (see Fig. 1):

1. simulation of snow cover conditions using measured weather data as input,
2. simulation of avalanches using initial conditions defined by snow cover conditions,
3. contingency table analysis to define the statistical score of avalanche runout calculation.

The procedure is applied to simulate 12 documented avalanche events, for which extensive field measurements are available, including measurements from airborne laser scans, drones and photography, and hand-held GPS devices. To determine how the procedure performs, we compare the area

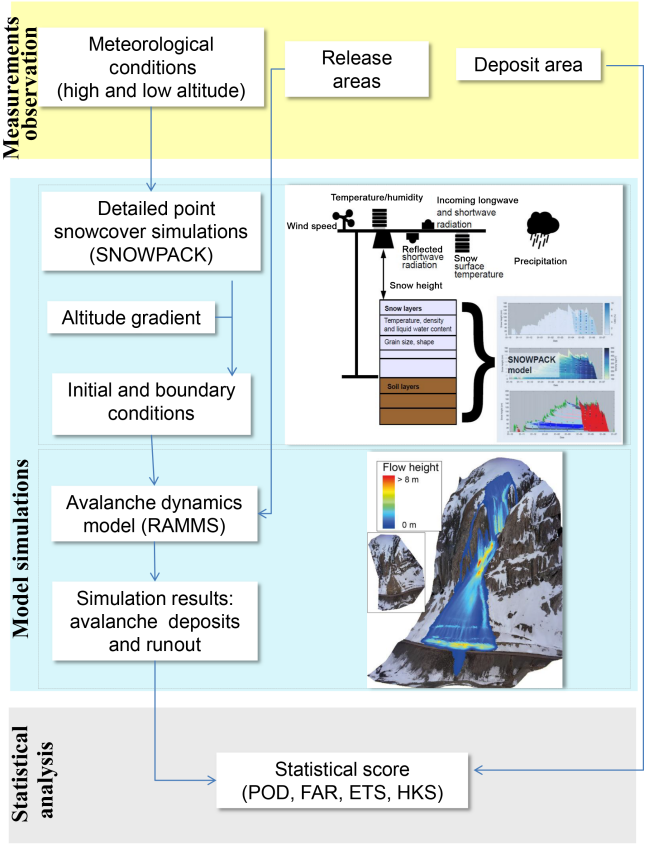

Figure 1. Flow diagram depicting the three-step model chain. The procedure begins by simulating snow cover conditions using measured weather data as input. Next, avalanche runout is simulated using initial and boundary conditions defined by snowpack modeling. Finally, a statistical score of the avalanche runout modeling is calculated.

covered in the simulations with the deposit area measured in the field. Simulated runout patterns are compared to field observations. The correspondence of observed deposits and calculated deposits is checked using a dichotomous contingency table, splitting the terrain into four different classes: hits, misses, false alarms and correct negatives.

Additionally, a sensitivity study is performed by interchanging the initial and boundary conditions of the 12 case studies and by varying the calculation grid cell size. The same contingency analysis and runout comparison are performed with the results obtained from the sensitivity analysis. This establishes to what extent the initial and boundary conditions indeed control the model performance.

2 Wet-snow avalanche modeling

Wet-snow avalanche modeling necessitates the simulation of four physical processes (Vera Valero et al., 2015, 2016):

1. the rise in avalanche temperature by frictional dissipation,
2. phase changes and the production of meltwater,
3. entrainment of snow mass *and* the associated internal (thermal) energy change of the avalanche,
4. constitutive models describing how the avalanche flow rheology changes as a function of temperature and moisture content.

One model that fulfils these requirements was developed by Vera Valero et al. (2015) andVera Valero et al. (2016).

2.1 Avalanche core

The flow of the dense avalanche core (subscript Φ) is described by nine independent state variables:

$$\mathbf{U}_\Phi = (M_\Phi, M_\Phi u_\Phi, M_\Phi v_\Phi, R_\Phi h_\Phi, E_\Phi h_\Phi, h_\Phi, M_\Phi w_\Phi, N_K, M_\mathrm{w})^T. \quad (1)$$

These variables include the core mass M_Φ (which contains both the ice mass *and* the water mass M_w); the flow height h_Φ; depth-averaged velocities parallel to the slope $\mathbf{u}_\Phi = (u_\Phi, v_\Phi)^T$, and, in the slope-perpendicular direction w_Φ, the sum of the kinetic and potential energies associated with the configuration and random movement of snow particles R_Φ and the internal heat energy (temperature) E_Φ. The formulation includes the dispersive pressure N_K (Buser and Bartelt, 2015; Bartelt et al., 2015).

The model equations can be written as a single vector equation:

$$\frac{\partial \mathbf{U}_\Phi}{\partial t} + \frac{\partial \mathbf{\Phi}_x}{\partial x} + \frac{\partial \mathbf{\Phi}_y}{\partial y} = \mathbf{G}_\Phi, \quad (2)$$

where the components ($\mathbf{\Phi}_x$, $\mathbf{\Phi}_y$, $\mathbf{G}_\Phi$) are

$$\mathbf{\Phi}_x = \begin{pmatrix} M_\Phi u_\Phi \\ M_\Phi u_\Phi^2 + \frac{1}{2} M_\Phi g' h_\Phi \\ M_\Phi u_\Phi v_\Phi \\ R_\Phi h_\Phi u_\Phi \\ E_\Phi h_\Phi u_\Phi \\ h_\Phi u_\Phi \\ M_\Phi w_\Phi u_\Phi \\ N_K u_\Phi \\ M_\mathrm{w} u_\Phi \end{pmatrix},$$

$$\mathbf{\Phi}_y = \begin{pmatrix} M_\Phi v_\Phi \\ M_\Phi u_\Phi v_\Phi \\ M_\Phi v_\Phi^2 + \frac{1}{2} M_\Phi g' h_\Phi \\ R_\Phi h_\Phi v_\Phi \\ E_\Phi h_\Phi v_\Phi \\ h_\Phi v_\Phi \\ M_\Phi w_\Phi v_\Phi \\ N_K v_\Phi \\ M_\mathrm{w} v_\Phi \end{pmatrix},$$

$$\mathbf{G}_\Phi = \begin{pmatrix} \dot{M}_{\Sigma\to\Phi} \\ G_x - S_{\Phi x} \\ G_y - S_{\Phi y} \\ \dot{P}_\Phi \\ \dot{Q}_\Phi + \dot{Q}_{\Sigma\to\Phi} + \dot{Q}_w \\ w_\Phi \\ N_K \\ 2\dot{P}_\Phi^V - 2N w_\Phi / h_\Phi \\ \dot{M}_{\Sigma\to w} + \dot{M}_w \end{pmatrix}. \quad (3)$$

The flowing avalanche is driven by the gravitational acceleration in the tangential directions $\mathbf{G} = (G_x, G_y) = (M_\Phi g_x, M_\Phi g_y)$. The model equations are solved using the same numerical schemes as outlined in Christen et al. (2010).

The model assumes nonzero slope-perpendicular accelerations and therefore calculates the slope-perpendicular velocity of the core w_Φ (Buser and Bartelt, 2015; Bartelt et al., 2015). The center of mass of the granular ensemble moves with the slope-perpendicular velocity w_Φ. When $w_\Phi > 0$, the granular ensemble is expanding; conversely when $w_\Phi < 0$, the volume is contracting. The densest packing of granules defines the co-volume height ${}^0h_\Phi^s$ and density ${}^0\rho_\Phi^s$ (Buser and Bartelt, 2015; Bartelt et al., 2015). The co-volume has the property that $h_\Phi^s \geq {}^0h_\Phi^s$ and $\rho_\Phi^s \leq {}^0\rho_\Phi^s$. The normal pressure at the base of the column N is therefore no longer hydrostatic but includes the impulsive reaction N_K associated with the slope-perpendicular accelerations (Bartelt and Buser, 2018):

$$N_K = M_\Phi \dot{w}_\Phi. \quad (4)$$

The total acceleration in the slope-perpendicular direction is denoted g'; it is composed of the slope-perpendicular component of gravity g_z, dispersive acceleration $\dot{w}_\Phi$ and centripetal accelerations f_z, (Fischer et al., 2012). The total normal force at the base of the avalanche is given by N:

$$N = M_\Phi g' = M_\Phi g_z + N_K + M_\Phi f_z. \quad (5)$$

Changes in density are induced by shearing: the shearing stress in the avalanche core $\mathbf{S}_\Phi$ induces particle trajectories that are no longer in line with the mean downslope velocities $\mathbf{u}_\Phi$ (Gubler, 1987; Bartelt et al., 2006). The kinetic energy associated with the velocity fluctuations is denoted R_Φ^K. The potential energy associated with the dilation of the core is denoted R_Φ^V.

The production of free mechanical energy $\dot{P}_\Phi$ is given by an equation containing two model parameters: the production parameter α and the decay parameter β (see Buser and Bartelt, 2009):

$$\dot{P}_\Phi = \alpha [\mathbf{S}_\Phi \cdot \mathbf{u}_\Phi] - \beta R_\Phi^K h_\Phi. \quad (6)$$

The production parameter α defines the generation of the total free mechanical energy from the shear work rate

$[\mathbf{S}_\Phi \cdot \mathbf{u}_\Phi]$; the parameter β defines the decrease of the kinetic part R_Φ^K by inelastic particle interactions. The energy flux associated with the configurational changes is denoted $\dot{P}_\Phi^V$ and given by

$$\dot{P}_\Phi^V = \gamma \dot{P}_\Phi. \tag{7}$$

The parameter γ therefore determines the magnitude of the dilatation of the flow volume under a shearing action. When $\gamma = 0$, there is no volume expansion by shearing. For wet-snow flows the value of γ is small, $\gamma < 0.2$. The basal boundary plays a prominent role because particle motions in the slope-perpendicular direction are inhibited by the boundary and reflected back into the flow. The basal boundary converts the production of random kinetic energy $\dot{P}_\Phi$ in the bulk into an energy flux that changes the z location of particles and therefore the potential energy and particle configuration of the core. The potential energy of the configuration of the particle ensemble is denoted P_Φ^V.

2.2 Avalanche temperature

We model-temperature dependent effects by tracking the depth-averaged avalanche temperature T_Φ within the flow (Vera Valero et al., 2015). The temperature T_Φ is related to the internal heat energy E_Φ by the specific heat capacity of snow c_Φ:

$$E_\Phi = \rho_\Phi c_\Phi T_\Phi. \tag{8}$$

The avalanche temperature is governed by (1) the initial temperature of the snow T_0, (2) dissipation of kinetic energy by shearing $\dot{Q}_\Phi$, (3) thermal energy input from entrained snow $\dot{Q}_{\Sigma\to\Phi}$ and (4) latent heat effects from phase changes $\dot{Q}_w$ (meltwater production); see Vera Valero et al. (2015). Dissipation is the part of the shear work not being converted into free mechanical energy in addition to the inelastic interactions between particles that is the decay of random kinetic energy, R_Φ^K.

$$\dot{Q}_\Phi = (1-\alpha)\,[\mathbf{S}_\Phi \cdot \mathbf{u}_\Phi] + \beta R_\Phi^K h_\Phi \tag{9}$$

A fundamental assumption of this model is that liquid water mass is bonded to the ice matrix of the snow particles and therefore is transported with the flowing snow. Mathematically, the governing equations treat moisture content as a passive scalar. Meltwater production is considered as a constraint on the flow temperature of the avalanche: the mean flow temperature T_Φ can never exceed the melting temperature of ice $T_\mathrm{m} = 273.15\,\mathrm{K}$. The energy for the phase change is given by the latent heat L,

$$\dot{Q}_w = L\dot{M}_\mathrm{w}, \tag{10}$$

under the thermal constraint such that within a time increment Δt

$$\int_0^{\Delta t} \dot{Q}_w \mathrm{d}t = M_\Phi c_\Phi (T_\Phi - T_\mathrm{m}) \quad \text{for} \quad T > T_\mathrm{m}. \tag{11}$$

Obviously, when the flow temperature of the avalanche does not exceed the melting temperature, no latent heat is produced; $\dot{Q}_w = 0$.

2.3 Snow entrainment

Another source of thermal energy is snow entrainment. The total mass that is entrained from the snow cover (Σ) is given by

$$\dot{M}_{\Sigma\to\Phi} = \rho_\Sigma \kappa \mathbf{u}_\Phi, \tag{12}$$

where ρ_Σ is the density of snow and κ the dimensionless erodibility coefficient. The value of the erodibility coefficient depends on snow quality. Values for warm, wet snow are reported in Vera Valero et al. (2015) and Vera Valero et al. (2016). The liquid water mass entrained by the avalanche is therefore

$$\dot{M}_{\Sigma\to w} = \theta_\Sigma^w \dot{M}_{\Sigma\to\Phi}, \tag{13}$$

where θ^w is the LWC of the entrained snow. The thermal energy entrained during the mass intake is

$$\dot{Q}_{\Sigma\to\Phi} = \left[\theta_\Sigma^i c_\mathrm{i} + \theta_\Sigma^w c_\mathrm{w} + \theta_\Sigma^a c_\mathrm{a} + \frac{1}{2}\frac{{\mathbf{u}_\Phi}^2}{T_\Sigma}\right] \dot{M}_{\Sigma\to\Phi} T_\Sigma, \tag{14}$$

where c_i, c_w and c_a are the specific heat capacity of ice, water and air, respectively. When the snow layer contains water $\theta_\Sigma^w > 0$, then the temperature of the entire layer is set to $T_\Sigma = 0\,^\circ\mathrm{C}$. Equation (14) takes into account the thermal energy contained in the entrained snow.

2.4 Flow friction

To model frictional resistance $\mathbf{S}_\Phi = (S_{\Phi x}, S_{\Phi y})$ in wet-snow avalanche flow, we apply a modified Voellmy model (Voellmy, 1955; Salm et al., 1990; Salm, 1993; Christen et al., 2010),

$$\mathbf{S}_\Phi = \frac{\mathbf{u}_\Phi}{\mathbf{u}_\Phi}\left[S_\mu + S_\xi\right], \tag{15}$$

consisting of both a Coulomb friction S_μ (coefficient μ) and a velocity dependent stress S_ξ (coefficient ξ). The friction terms S_μ and S_ξ are given by

$$S_\mu = \mu N - (1-\mu) N_0 \exp\left(\frac{N}{N_0}\right) + (1-\mu) N_0 \tag{16}$$

and

$$S_\xi = \rho_\Phi g \frac{{\mathbf{u}_\Phi}^2}{\xi}. \tag{17}$$

In the Coulomb friction term, N_0 is the cohesion; see Bartelt et al. (2015) for values of N_0 for wet snow. The form of Eq. (16) ensures that the shear stress $S_\mu = 0$ when $N = 0$, in accordance with shear and normal force measurements in

snow chute experiments (Platzer et al., 2007). To model the decrease in friction from meltwater lubrication, we make the Coulomb stress dependent on the meltwater water content h_w. We use the following lubrication function to replace the standard Coulomb friction coefficient μ:

$$\mu(h_w) = \mu_w + (\mu_d - \mu_w) \exp\left[-\frac{h_w}{h_s}\right], \quad (18)$$

where μ_d is the dry Voellmy friction coefficient, μ_w is the limit value of lubricated friction (Voellmy assumed this value to be $\mu_w = 0$ in the limiting case) and h_s is a scaling factor describing the height of the shear layer where meltwater is concentrated. The dry friction μ_d depends on the avalanche configuration:

$$\mu_d = \mu_0 \exp\left[-\frac{R_\Phi^V}{R_0 + N_0}\right], \quad (19)$$

where μ_0 is the dry Coulomb friction associated with the flow of the co-volume, which we take to be $\mu_0 = 0.55$; see Buser and Bartelt (2015). The parameter R_0 defines the activation energy for fluidization. Cohesion enhances the activation energy and therefore hinders the fluidization of the avalanche core (Bartelt et al., 2015).

3 Selected wet-snow avalanche events and modeling procedure

We apply the numerical model to simulate documented wet-snow avalanches. The data set includes 12 wet-snow avalanches that occurred in the Swiss Alps and in the Chilean Central Andes between 2008 and 2015. The avalanches were selected for three reasons: (1) the avalanche was located in the vicinity of an automatic weather station (henceforth AWS); (2) the release area and the area inundated by the avalanche were measured by hand-held GPS, drone or terrestrial laser scanning; and (3) a high-resolution digital elevation model (DEM; i.e., 2 m or higher) is available to simulate the terrain. This information is summarized in Table 1. The avalanche release volumes varied between 7000 and 330 000 m^3. Most avalanches released from a wet snow cover and entrained additional wet snow. However, in three events (Grengiols, Braemabuhl Verbauung and Gatschiefer) the avalanche released as a dry slab at subzero temperatures but entrained warm, moist snow at lower elevations. The release, transit and deposit zone of 10 of the 12 case studies were additional photographed from a helicopter. The two remaining avalanches (Drusatscha and Braemabuhl, 2013) were photographed by the authors from the deposition zone. The measurements from the release areas and deposit outlines for every avalanche path are shown in Supplement A in the online supplement.

3.1 SNOWPACK simulations

The data provided by the automatic weather stations allow us to run detailed, physics-based snow cover simulations. We apply the SNOWPACK model (Bartelt and Lehning, 2002; Lehning et al., 2002; Wever et al., 2014) in a similar setup to that of the snow-height-driven simulations in Wever et al. (2015, 2016). Because SNOWPACK is a one-dimensional model, we must transfer point simulation results to the slope in order to apply a two-dimensional avalanche dynamics model operating in three-dimensional terrain. The horizontal distance between release zone or deposits zone and the meteorological station varied between 200 m (the nearest) and 2200 m (the farthest). More important than the linear distance is the difference in altitude. The elevation differences between the release zones or deposits zones and the weather stations (see Table 1) are typically less than 200 m, which we consider sufficiently small, given typical lapse rates in the atmosphere, to provide representative snow cover simulations to estimate the initial and boundary conditions of the case studies (Vera Valero et al., 2016; Wever et al., 2016).

To determine the initial temperature and moisture content of the snow cover requires an accurate modeling of the surface energy fluxes (sensible and latent heat exchanges, incoming short- and longwave radiation), which are influenced by the slope exposition. We account for exposition effects on surface energy fluxes in the release zones using the virtual slope concept proposed by Lehning and Fierz (2008), which was found to provide accurate slope simulations that correspond with wet-snow avalanche activity (Wever et al., 2016; Vera Valero et al., 2016). We obtain snow cover layering, temperature, density and LWC in the release zones using virtual slope angles of 35° (see Table 2). The real slope angles of the release zones varied between 32 and 45°. Shortwave radiation measured at the AWS as well as snowfall amounts are re-projected onto these slopes, taking into account the exposition of the slope (Lehning and Fierz, 2008).

For a few cases, field measurements using drones or laser scanning allowed for an estimate of the fracture height. For the Gruenbodeli case, a fracture height of 0.70 m has been determined from the field measurements. Given a slope angle of 35°, this translates to a perpendicular fracture height of 0.57. SNOWPACK provides a slope-perpendicular fracture height of 0.56 m here, based on the position of the highest water accumulation. Similarly, for the Salezer and Gatschiefer case, an observed fracture height of 1.1 m (0.90 m slope perpendicular) and 2.0 m (1.64 m slope perpendicular) is found, respectively, which was estimated by SNOWPACK to be 0.95 and 1.72 m slope perpendicular, respectively. All these cases occurred on the same day, and the SNOWPACK simulations clearly correctly identify fracture heights for these cases. Similarly, for the Braemabuhl Wildi and CV-1 case, a fracture depth of 1.1 m (0.90 m slope perpendicular) was determined from drone measurements. The SNOWPACK simu-

Table 1. List of case studies with date and estimated time of occurrence. The designation for the automatic weather station (AWS) in the release zone contains the nearest weather station followed by the exposition and altitude. The AWS at the bottom of the valley was used to characterize the deposit area. The column "Fracture" contains the method used to determine the location and height of the released snow mass. For the more accurate laser scan and drone measurements, the measured mean fracture heights are additionally provided.

Avalanche	Date/time	AWS release (altitude in m)	AWS valley (altitude in m)	Fracture method/height (m)	Altitude release deposits (m)
Gruenbodeli	23/04/2008 ≈ 14:00	KLO2-NE (2140)	SLF2 (1550)	Laser scan / 0.70	1900/1600
Salezer	23/04/2008 15:00	WFJ2-W (2560)	SLF2 (1550)	Laser scan/1.1	2400/1500
Gastschiefer	23/04/2008 16:00	KLO3-N (2310)	SLF2 (1550)	Laser scan/2.0	2400/1200
Braemabuhl 2013	18/04/2013 15:00	WFJ2-NE (2560)	SLF2 (1550)	GPS profile	2200/1600
Drusatcha	15/04/2013 17:00	WFJ2-W (2560)	SLF2 (1550)	GPS profile	2200/1700
MO-4 Andina Chile	15/10/2013 19:15	CAND5-SE (3520)	Lagunitas (2770)	Ortophoto	3700/3200
Grengiols	26/12/2013 13:00	GOMS-NE (2450)	Estimated	GPS profile	2300/1400
Verbier Mont Rogneux	13/03/2014 17:00	ATT2-W (2545)	Estimated	GPS profile	2400/1700
Verbier Ba Comb	13/03/2014 17:00	ATT2-SW (2545)	Estimated	GPS profile	2200/1600
Braemabuhl verbauung	03/04/2015 12:00	WFJ2-NE (2560)	SLF2 (1550)	GPS profile	2200/1600
Braemabuhl Wildi	04/04/2015 ≈ 14:00	WFJ2-NE (2560)	SLF2 (1550)	Drone/1.1	2200/1600
CV-1 Andina Chile	19/10/2015 17:00	CAND5-E (3520)	Lagunitas (2770)	Drone/1.1	2700/2500

lations provide a slope-perpendicular fracture height of 1.10 and 0.95 m, respectively.

To describe the snow cover at lower elevations in the transit and runout zones, we used the simulated snow cover based on meteorological data measured at a station at the bottom of the valley. In this case, flat-field simulations were analyzed, as deposits zones of large avalanches are often in relatively flat terrain, compared to the release zones. The simulated snow cover information provides us with the snow temperature, snow height, density and LWC at lower elevations. In 8 of the 12 case studies, the snow cover in the avalanche model can be considered as a single homogeneous layer, while for the remaining case studies the snow cover was best modeled as a two-layer system consisting of old wet snow covered by dry new snow; see Table 3. The elevation-dependent properties of the snow cover along the avalanche path were determined by constructing a linear gradient between the upper and lower meteorological stations. This procedure could be applied for the case studies that occurred near Davos (seven case studies) and the cases in Chile (two cases).

For the remaining case studies (Verbier Mont Rogneux, Verbier Ba Combe and Grengiols) we estimated snow cover conditions along the avalanche track by applying a negative linear gradient of one-third of the snow cover height per 1000 m of altitude. This rule provides gradients of snow cover height of 2 to 6 cm per 100 m of elevation (see Table 3). This method is in agreement with the Hydrological Atlas of Switzerland. In these special cases, the snow temperature, density and LWC were kept constant to the values estimated by the SNOWPACK model at the release altitude. In the case of avalanches with new snow on top of the wet old snow cover, we consider the new snow amount measured at the AWS and estimate a decreasing linear gradient of new snow height with altitude.

3.2 Avalanche dynamics calculations: initial and boundary conditions

We apply two different models to simulate the 12 case studies. The first is based on the thermomechanical avalanche dynamics equations presented in Sect. 2 (see Vera Valero et al., 2015, 2016); the second avalanche model follows the Swiss guidelines on avalanche calculation (Salm et al., 1990; Christen et al., 2010). The numerical model is outlined in Gruber and Bartelt (2007). Both models are implemented in the RAMMS (RApid Mass MovementS) software. Models and model parameters are compared in Table 4.

In the calculations, we are primarily concerned with the initial and boundary conditions, which are given by the snow cover model simulations; the release area is given by the field measurements. The fracture height is defined by the location of the highest water accumulation within the snow cover (Wever et al., 2016) as was previously suggested by Vera Valero et al. (2016). Once the fracture height is known, we set the snow density, snow temperature and liquid water values as the mean values over the slab which extends from the location of the maximum liquid water to the snow surface. We take the values at the estimated time of avalanche release. These values are shown in Tables 2 and 3. The amount of erodible snow is also calculated using the location of the ponding layer. However, we calculate a gradient between the snow cover conditions at the release and the conditions at the bottom of the valley. This means that the depth of the fracture height and erodible layer decreases with elevation. The erosion model used is described by Christen et al. (2010) and Bartelt et al. (2012a).

Once the initial and boundary conditions were found, the first set of simulations using the extended model was performed. As input parameters, the model uses the release area (measured), the snow cover initial conditions (calculated),

Table 2. Initial conditions derived from SNOWPACK simulations at the release for each avalanche.

Avalanche	Date/time	Meteostation stations	LWC (%)	Height (m)	Density (kg m^{-3})	Temperature (°C)	Cohesion (Pa)	Released volume (m^3)	Growth index (–)
Gruenbodeli	23/04/2008 ≈ 14:00	KLO3-NE	1.45	0.56	197	−0.3	100.0	52882	2.2
Salezer	23/04/2008 ≈ 15:00	ATT2-SW	1.89	0.95	317	−0.1	150.0	46 394	2.4
Gatschiefer	23/04/2008 16:00	KLO3-N	1.63	1.72	320	−0.1	150.0	330 544	1.8
Braemabuhl 2013	18/04/2013 15:00	WFJ2-NE	2.97	1.11	353	0.0	150.0	21 404	3.5
Drusatscha	15/04/2013 17:00	WFJ2-W	3.41	0.54	291	0.0	150.0	32 730	2.3
MO-4 Andina Chile	15/10/2013 19:15	CAND5-SE	2.44	0.90	296	−0.2	150.0	9257	2.1
Grengiols	26/12/2013 ≈ 13:00	GOMS-NE	0.00	1.10	175	−7.4	100.0	129 392	3.9
Verbier Mont Rogneux	13/03/2014 17:00	ATT2-W	3.67	0.60	317	0.0	150.0	55 817	1.8
Verbier Ba Combe	13/03/2014 17:00	ATT2-SW	3.40	0.58	349	0.0	150.0	21 349	2.1
Braemabuhl verbauung	03/04/2015 12:00	WFJ2-NE	1.01	1.10	285	0.0	150.0	6858	2.7
Braemabuhl Wildi	04/04/2015 ≈ 14:00	WFJ2-NE	1.23	1.10	245	−1.4	100.0	45 614	3.3
CV-1 Andina Chile	19/10/2015 17:00	CAND5-E	2.36	0.95	359	−0.1	150.0	4019	2.2

Table 3. Erosion conditions derived from the snow cover simulations for each avalanche case study. Upper and lower denotes two different erosion layers. The two-layer system was used when new snow was lying over old snow cover and both layers were part of the studied avalanche. In the case of only one layer, all the fields at the second, lower layer are set to zero.

	LWC (%)		Erosion height (m)		Erosion height gradient (m per 100 m)		Density (kg m^{-3})		Vol water (mm m^{-1})		Temperature (°C)		Temperature gradient (°C per 100 m)		Erodibility (–)	
Avalanche	Upper	Lower	Upper	Lower	Upper	Lower	Upper	Lower	Upper	Lower	Upper	Lower	Upper	Lower	Upper	Lower
Gruenbodeli	1.45	–	0.56	0.00	0.02	–	197	–	8.1	–	–0.2	–	0.0	–	0.8	–
Salezer	1.89	–	0.95	0.00	0.03	–	317	–	18.0	–	0.0	–	0.0	–	0.7	–
Gatschiefer	0.00	1.47	0.55	0.95	0.03	0.04	185	360	0.0	14.0	–1.0	0.0	0.0	0.0	0.6	0.7
Braemabuhl 2013	2.97	–	1.11	0.00	0.04	–	353	–	33.0	–	0.0	–	0.0	–	0.6	–
Drusatscha	3.41	–	0.54	0.00	0.02	–	291	–	18.4	–	0.0	–	0.0	–	0.6	–
MO-4 Andina Chile	2.44	–	0.90	0.00	0.03	–	296	–	22.0	–	0.0	–	0.0	–	0.6	–
Grengiols	0.00	4.67	0.43	0.60	0.03	0.00	175	270	0.0	28.0	–7.4	0.0	1.5	0.0	0.7	0.8
Verbier Mont Rogneux	3.00	–	0.60	0.00	0.02	–	317	–	18.0	–	0.0	–	0.0	–	0.6	–
Verbier Ba Combe	2.59	–	0.58	0.00	0.02	–	349	–	15.0	–	0.0	–	0.0	–	0.6	–
Braemabuhl verbauung	0.00	1.41	0.25	0.85	0.00	0.04	158	335	0.0	12.0	–2.0	0.0	0.0	0.0	0.8	0.8
Braemabuhl Wildi	0.00	1.25	0.30	0.80	0.00	0.03	164	335	0.0	10.0	–2.0	0.0	0.0	0.0	0.6	0.6
CV-1 Andina Chile	1.51	–	0.37	0.00	0.00	–	359	–	5.6	–	−0.1	–	0.0	–	0.6	–

and a set of friction and avalanche parameters. The avalanche parameters were found by Buser and Bartelt (2009), Vera Valero et al. (2015) and Buser and Bartelt (2015). These parameters were kept constant for all 12 case studies as in Vera Valero et al. (2016). The fluidization parameters α and γ (see Bartelt et al., 2006; Vera Valero et al., 2016) are fixed to pre-determined values based on the terrain characteristics for each avalanche path. Once these parameters are fixed, they are not tuned for the remaining set of simulations. All simulations were carried out using a grid resolution of 3 m except for the CV-1 case, where the confined and gullied terrain was found to require a higher grid resolution of 1 m.

To perform standard Voellmy-Salm snow avalanche simulations following the Swiss guidelines (Salm et al., 1990), it is necessary to include the entire avalanche mass within the release volume. The guidelines do not consider entrainment along the avalanche path, and therefore erosion was not considered in the Voellmy-Salm simulations. This procedure was adopted to follow as closely as possible the Swiss guideline procedures for avalanche calculations and allows a comparison between models which consider entrainment conditions (extended model) and models which employ calibrated parameters (Voellmy-Salm). The avalanche mass of the release area was estimated from the final mass (released plus eroded) calculated using the extended model. The total mass calculated in the extended model is concentrated in the measured release area. With this approach, a higher fracture height is obtained than in model calculations with entrainment. This method ensures that the total mass in both simulations is similar. The Swiss guidelines provide the user a set of friction parameters to use depending on the avalanche size and avalanche return period. Those friction parameters correspond to extreme, fast-moving, dry-flowing avalanches, which have longer runouts than wet ones. For the 12 case studies, the friction parameters used are the ones corresponding to the class "small" avalanches and a return period of 10 to 30 years. This parameter combination led to the overall best fit to observations. The calculations were performed with the same terrain and grid resolution.

3.3 Contingency table analysis for deposition area

The results obtained with the two models are compared through a statistical contingency table analysis. We compare the area covered by the avalanche deposits calculated with both models with the deposit area measured for each case study. The terrain is divided into squared cells which correspond with the calculation cells used in the avalanche simula-

Table 4. Overview of model and model parameters used to simulate the 12 case studies.

	Guidelines-VS	Thermomechanical	Comments
Reference	Salm et al. (1990) Gruber and Bartelt (2007)	Vera Valero et al. (2015, 2016); Buser and Bartelt (2015)	Both models in RAMMS; Christen et al. (2010)
μ_0 (–)	Calibrated/guidelines	0.55	Reduced by lubrication
μ_w (–)	None	0.12	Constant in all simulations
ξ_0 ($\mathrm{m\,s^{-2}}$)	Calibrated/guidelines	1300	Reduced by fluidization
N_0 (Pa)	200	200	Measured; see Bartelt et al. (2015)
α (–)	0.00	0.05–0.07	Depends on roughness
β ($1\,\mathrm{s^{-1}}$)	None	1.0	Depends on temperature
R_0 ($\mathrm{kJ\,m^{-3}}$)	None	2	Constant in all simulations
h_m (m)	None	0.1	Size of lubricated layer
κ (–)	None	0.6–0.8	VS guidelines no entrainment

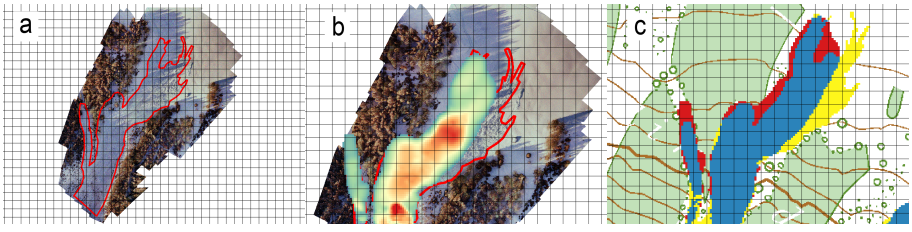

		Observed		
		Yes	**No**	**Total forecasted**
Forecasted	**Yes**	Hits	False alarms	Forecasted yes
	No	Misses	Correct negatives	Forecasted no
	Total observed	Observed yes	Observed no	**TOTAL**

Figure 2. Method to construct the contingency table, based on measured deposits outline **(a)**, which is then combined with the simulated deposit area **(b)** to identify hits (blue), false alarm (red), misses (yellow) and correct negatives (no color, map only) **(c)**.

tions (see Fig. 2a and b). For each cell we check whether the cell was covered by the observed avalanche deposits or not and whether the cell was covered by the avalanche simulation once the simulation stops or not. A cell will be considered as covered by the avalanche simulations only if the calculated flow height with the mass at rest is more than 20 cm, corresponding approximately to two granules in diameter (Bartelt and McArdell, 2009). Variations in modeled and observed deposition heights are not captured with this procedure. The calculated flow height at the last calculation step provides us with the inundation area. These flow heights might not represent the observed deposition depth, which is governed by different deposition mechanisms. The correspondence of observed and calculated inundation area is checked using a dichotomous contingency table (see Fig. 2) that splits the terrain into four different classes: hits, misses, false alarm and correct negatives (see Fig. 2c). Computing the amount of cells for each class allows us to calculate different metrics to judge how both models perform. In this study the probability of detection (POD), false-alarm rate (FAR), equitable threat score (ETS) and Hanssen–Kuipers skill score or true skill statistic (HKS) (see Table 5) are calculated (Woodcock, 1976). For POD, ETS and HKS a score of 1 would mean a perfect score; in the case of FAR a score of 0 would indicate a perfect score. These two-dimensional procedures avoid the problem of defining a one-dimensional measure of avalanche runout.

3.4 Avalanche runout

In addition to the contingency analysis study for the inundated area, runout distance in analyzed. The runout distance was calculated from the difference in meters between the maximum distance reached by the avalanche in the measurements and the avalanche simulation calculated over the line of steepest descent for each avalanche path in a DEM smoothed to a resolution of 20 m (see Fig. 3). The line of

Table 5. Mathematical definition of the statistics scores: probability of detection (POD), false-alarm rate (FAR), equitable threat score (ETS) and Hanssen–Kuipers score or true skill statistic (HKS).

$\mathrm{FAR} = \frac{\text{false alarms}}{\text{hits} + \text{false alarms}}$	$\mathrm{POD} = \frac{\text{hits}}{\text{hits} + \text{misses}}$
$\mathrm{HKS} = \frac{\text{hits}}{\text{hits} + \text{misses}} - \frac{\text{false alarms}}{\text{false alarms} + \text{correct negatives}}$	$\mathrm{ETS} = \frac{\text{hits} - \text{hits}_{\text{random}}}{\text{hits} + \text{misses} + \text{false alarms} - \text{hits}_{random}}$ *

* where $\text{hits}_{\text{random}} = \frac{(\text{hits}+\text{misses})(\text{hits}+\text{false alarms})}{\text{total}}$.

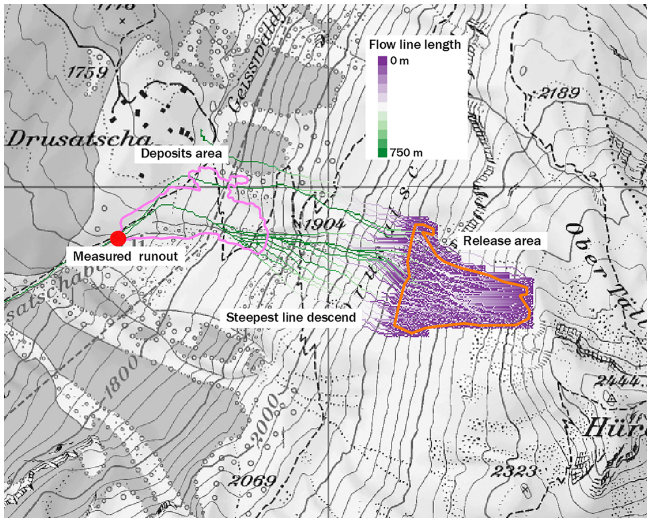

Figure 3. Runout distance calculation procedure. From each calculation cell at the release area the line of steepest descent is calculated. The intersection of the lowest part of the avalanche deposits with the longest calculated flow line (red dot) define the avalanche runout. The same procedure is repeated with the simulation results. The distance measured on the steepest line between the two intersection points is defined as the runout calculation error.

steepest descent was chosen as the longest line of steepest descent among all the possible ones departing from the depicted release area for each avalanche path. All simulations stopped when the avalanche simulation contained less than 5 % of the maximum calculated momentum (Christen et al., 2010).

3.5 Influence of initial conditions on avalanche runout: sensitivity study

In addition to using an avalanche dynamics model where snow temperature and wetness directly influence the flow rheology, we use a novel approach here to use simulated snow cover conditions to directly drive the avalanche dynamics model. We constructed a sensitivity study (i) to investigate the influence of initial snow cover conditions on the simulated avalanches and (ii) to investigate if the snow cover simulations by the SNOWPACK model for a specific case add information. We consider the 12 case studies to represent 12 individual cases of wet-snow avalanches. We construct the members of the sensitivity study by interchanging the initial conditions from the 12 case studies. This way, we ensure realistic and self-consistent simulated snow cover results which represent real wet-snow avalanche cases, in contrast with when individual variables would be varied one by one. Furthermore, we consider that, for the avalanche dynamics simulations, the snow cover conditions can be separated meaningfully in mass of the slab on the one hand (given by slab height and snow density), and temperature and LWC on the other hand.

For the study, three sets of simulations were constructed as follows:

1. Twelve simulations for each avalanche path interchanging the initial and boundary conditions (fracture and erosion height, snow temperature, density and LWC at the erosion and at the release) for the 12 different avalanches, thereby obtaining a set of 144 simulations.

2. A second set of simulations were performed by using the snow temperature and LWC that was simulated by the snow cover model for that track. However, we varied the release and erosion heights and the snow density of the 12 different case studies. This set contains another 144 simulations and is used to verify the model sensibility to changes in avalanche mass at the release and at the erosion.

3. A third set of simulations is constructed by keeping the snow heights and snow densities constant. The remaining conditions (i.e., temperature and LWC) were taken from the 12 case studies, leading to another set of 144 simulations, to investigate the importance of snow cover properties in relation to snowpack mass.

Consequently, for each of the 12 case studies we performed three different sets of simulations, resulting in a total of 432 simulations ($3 \times 12 \times 12$) where we interchanged the initial and boundary conditions from the 12 different initial and boundary conditions. For each simulation, we determined the difference between the observed and simulated runout as well as the contingency scores for the inundated area.

4 Results

The contingency table analysis is used to explore the following questions:

1. Is it possible to drive avalanche dynamics calculations with initial and boundary conditions derived from snow cover modeling? Does the application of thermomechanical models improve the area covered by avalanche deposits and runout distances?
2. How sensitive are the simulated deposit areas and runout distances to released mass and snow cover properties?
3. What role does the calculation grid resolution play in the simulated areas covered by the deposits and runout distances?

The results of the model runs are presented extensively in the paper's supplement. The graphs in Supplement A facilitate a direct comparison between the thermomechanical approach, the standard Voellmy-Salm procedure and the actual avalanche measurements, including the location of the deposits with respect to the observed release zone. Supplement B contains the results of the model permutations. This graphical output enables a quick assessment of the model sensitivity. In the following we statistically analyze model performance.

4.1 Comparison between the guideline-VS and the thermomechanical model

The 12 avalanche events were simulated using the guideline-VS model (Salm et al., 1990) and the thermomechanical wet-snow avalanche model presented in Sect. 2. Recall that the guideline friction parameters were used for wet-snow avalanches and that best overall fit to the observed inundation areas was found using the classification small and frequent return period of 10–30 years. The thermomechanical model used the fracture and entrainment heights derived from the snow cover modeling. Bulk snow temperature and moisture contents were determined by layer averaging of the fracture height. The contingency table analysis for deposition areas and runout distances is shown in Fig. 4.

A comparison between the guideline-VS and the wet-snow avalanche model reveals that the thermomechanical model obtains significantly better results than the guideline-VS model. The POD in conjunction with FAR scores achieved by the thermomechanical model improves the results by more than 0.15 points (see Fig. 4). The ETS achieved by the thermomechanical model improves the guideline procedure by 0.13 points (see Fig. 4). Additionally, the HKS reached by the thermomechanical model improves by 0.17 points in comparison to the HKS reached by the guideline model. Therefore, the thermomechanical model statistically outperforms the guideline procedure in all four contingency metrics.

The difference in performance between guideline-VS and thermomechanical wet-snow avalanche model simulations differs per avalanche path (see Fig. 4). The guideline-VS procedure has particular difficulties with tracks containing a smooth transition between the acceleration and deposition zones. These avalanche paths have a long distance where the steepness gets progressively flatter (i.e., Braemabuhl, Mont Rogneux, Ba Combe and Drusatcha; see the online supplement). In contrast, the guideline-VS model does much better on avalanche paths with a sharp transition between the acceleration and runout zones (Gruenbodeli, Salezer and Gatschiefer). In the examples where the slope angle changes smoothly the guideline calculations systematically overran the measured deposits (Braemabuhl, Wildi, Mont Rogneux, Ba Combe). Thus, the guideline-VS does achieve good scores on detection (POD) but at the same time exhibits a high FAR.

The thermomechanical model performs equally well on both types of slope and is able to reproduce runout distances on slopes with gradual transition to the runout zone. In the case of Grengiols, the runout distance is somewhat underestimated; however, this was found to be caused by the uncertainty of the elevation of the snowfall limit. This is an important result since it indicates that the snow cover modeling must be able to accurately predict the snow line elevation.

4.2 Sensitivity analysis

The scores of the contingency table analysis reveal that the thermomechanical model, which utilizes the modeled initial and boundary conditions, can outperform a model based on calibrated guideline friction parameters. The primary result of the preceding section is that guideline-based avalanche dynamics models with calibrated friction parameters (avalanches with return periods greater than 10 years) will have difficulty reconstructing individual case studies and that they are not easily linked to snow cover conditions. The next step is to check how sensitive the thermomechanical model is to changes in the simulated initial and boundary conditions.

4.2.1 Role of initial conditions

To demonstrate the role of initial conditions, we simulated the 12 case studies using the initial conditions of all the other case studies, creating a total of 144 permutations. The initial conditions consist of fracture height, snow density, temperature and LWC. For example, we simulated the Ba Combe case study with the initial conditions from the other 11 case studies. The simulation results of every one of the permutations for each avalanche path are shown in Supplement B in the online supplement.

Figure 5 depicts the results of the 144 simulations. In these plots, the red dots indicate the simulations performed with the SNOWPACK-modeled initial conditions belonging to the

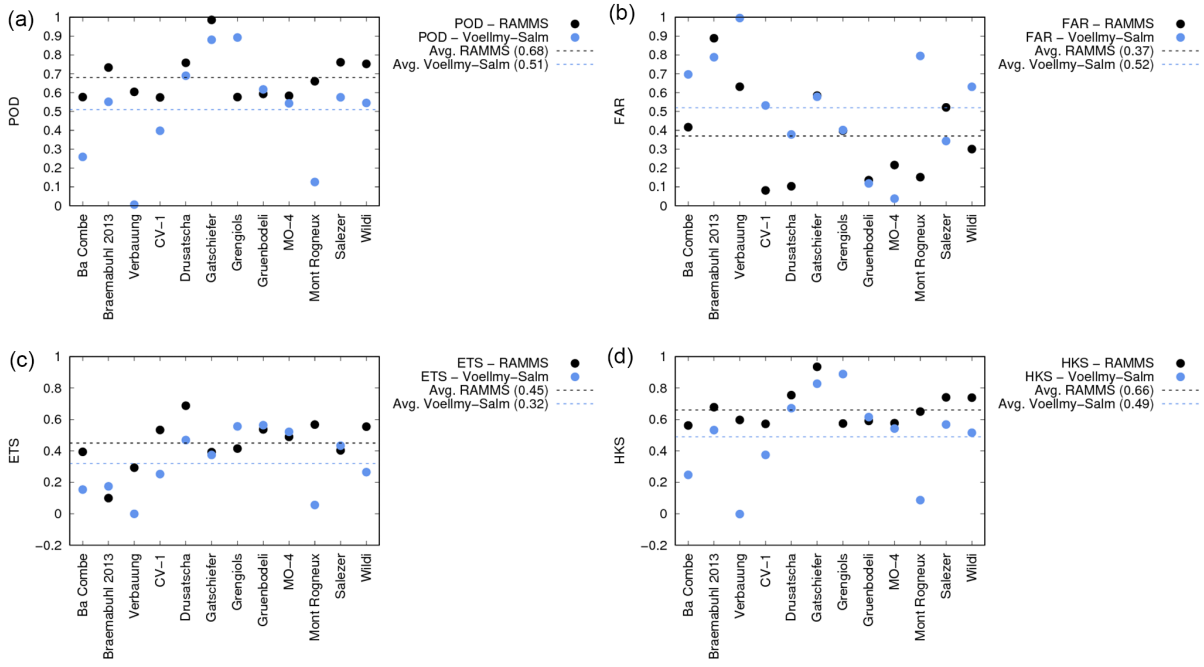

Figure 4. Comparison of the statistical results from the thermomechanical model RAMMS (black) and the guideline-VS model (blue), for POD **(a)**, FAR **(b)**, ETS **(c)** and HKS **(d)**.

specific avalanche path; the small black dots represent the remaining combinations of 11 simulations. The large open circle represents the average of the 11 permutations.

The first result of this sensitivity analysis is that the score difference varies by more than 0.2 statistical points for every avalanche path and indicator (POD, FAR, ETS and HKS scores). This result indicates a large variability of the model with different initial conditions. The POD scores using the "right" initial conditions are higher than using those from the other case studies. Furthermore, the FAR is lower. The average of the four statistical indicators calculated with the real initial and boundary conditions (red line in Fig. 5) outperformed the calculations with the interchanged initial and boundary conditions for every case study. However, for particular cases, simulations with initial conditions from another avalanche path outperformed the one calculated with the real initial conditions. A last important observation is that the spread of scores provided by the permutations of the initial conditions exceeds the spread of scores for all 12 simulations with the real initial conditions.

Again, for the longer avalanche paths with a smooth transition to the runout zone (Gatschiefer, Drusatcha, Grengiols, Verbier Mont Rogneux and Braemabuhl), the scores varied up to 0.5 points in comparison to avalanche paths where the transition is marked by an abrupt change in slope angle (MO-4, CV-1 and Gruenbodeli). Thus, long avalanche tracks with a smooth transition to the runout zone benefit the most from a correct initialization using SNOWPACK simulations.

4.2.2 Role of snow cover mass and density

The initial conditions include both mass/density and temperature/water content. To quantify the relative importance of initial mass versus initial snowpack properties, we performed another set of 144 simulations where only the mass (both the fracture mass and entrainment heights) varied. The results of the contingency table analysis are depicted in Fig. 6. The results are similar to the first sensitivity analysis, where the entire set of initial and boundary conditions were varied. This suggests that the selection of the initial and boundary conditions for mass is more important than for temperature/LWC. For wet-snow avalanches, this implies that the layers where meltwater accumulates in the release zone must be identified accurately as this defines the height of the fracture slab and therefore the release mass. A change in the fracture height of 10 cm can lead to a large variability in the predicted avalanche runout. This is a problematic result because it indicates the critical role of fracture height as an input parameter in avalanche simulations.

4.2.3 Role of snow cover temperature and water content

Figure 7 displays the results of the other set of 144 thermomechanical model simulations where the temperature and LWC in the release and entrainment zones were permuted. The mass (release and eroded) was defined by the snow cover simulations driven by the meteorological data for each case study. The statistical results are less sensitive to changes in

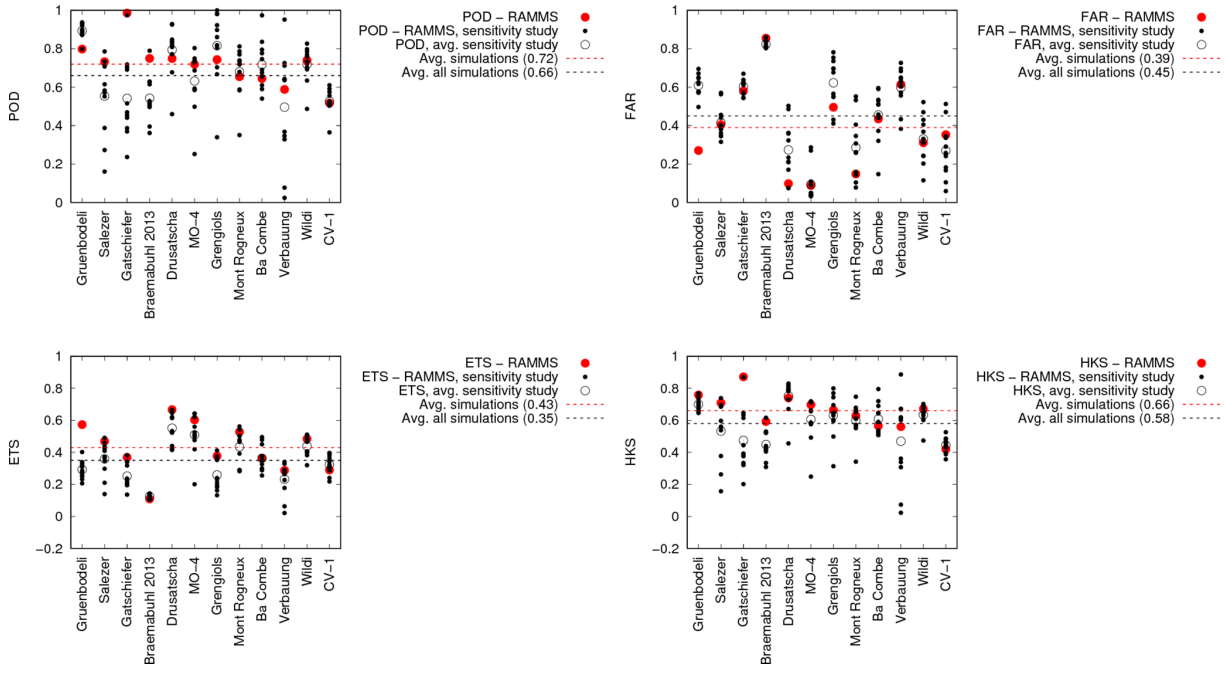

Figure 5. Sensitivity study simulating every avalanche path with the 12 different initial and boundary conditions using the thermomechanical model RAMMS. The red dot denotes the simulation performed with the initial and boundary conditions calculated for the corresponding avalanche path. The open black circle denotes the average of the 11 permutations (filled black dots). In this plot for every avalanche path fracture and erosion height, temperature, density and LWC at the release and along the avalanche path (erosion) are varied.

temperature and LWC than to mass. This is due to the fact that only wet-snow avalanches were considered, and the temperature range did not vary outside the wet-snow regime. This too is a reasonable result because moisture contents in the 12 case studies varied only between 0 and 5 %; see Table 3. Although the variations are less pronounced than those caused by mass changes, Fig. 7 illustrates that correctly specifying initial snow temperature and LWC also contributes positively to the model performance. The strong variation on long avalanche tracks with a smooth transition to runout zone demonstrates, once again, that path geometry dominates over changes in snow cover boundary conditions.

4.3 Sensitivity to calculation grid size

Contingency table scores for the thermomechanical model can also depend on the selected grid resolution. This would imply that the constant set of friction parameters of the wet-snow model is bounded to a particular cell size. We subsequently repeated the simulations using three different grid sizes: 3×3, 5×5 and 10×10 m. The influence on the contingency scores is depicted in Figs. 8 and 9 for 10 and 5 m, respectively.

A similar analysis was performed by Bühler et al. (2011), albeit without a statistical score and only on a limited number of case studies. The qualitative results of that study indicate that a coarser resolution smooths the terrain, causing the wet model simulations to overflow the observed deposit areas. Due to overflowing, the POD score increases by almost 0.1 statistical points on average in comparison with the 3 m resolution simulations. The coarser simulations are highly penalized in the FAR indicator, showing a drop of 0.2 statistical points on average in comparison with the finer resolution. The statistical scores (ETS and HKS) were positively influenced by the increase in hit rate, but this was compensated by the even larger increase in false alarms. The ETS score is severely penalized, dropping the statistical score by 0.15 points for the coarser simulations (10 m) in comparison to finer simulations (3 m). Even though the HKS score is more weighted to the number of hits, it likewise decreased, but by a smaller amount. The increase in false alarms was so large that it mostly compensated the improvement obtained by an increase in the number of hits.

The same analysis was repeated using 5 m resolution. In this case, the results do not differ greatly from the results obtained with a 3 m resolution. The 5 m resolution overall statistics (see Fig. 9) are close or even equal (in the case of the HKS score; see Fig. 5) to the results obtained by the 3 m resolution simulations. Nevertheless, the 5 m resolution simulations obtained not only a higher POD score than the 3 m resolution but also a higher FAR score. This pattern was already observed in the comparison between 3 and 10 m; however, in this case the difference is much lower. In the other two statistical indicators, ETS and HKS, even more similar results are obtained. The ETS score (see Fig. 9) is slightly lower

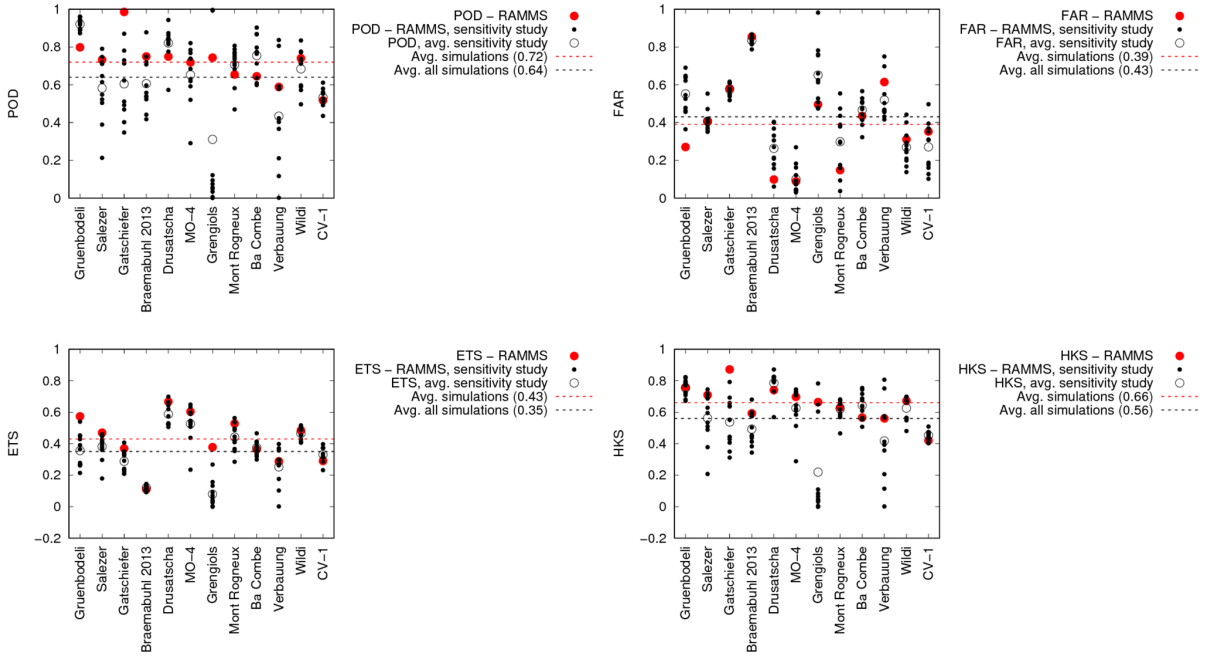

Figure 6. Sensitivity of the thermomechanical model RAMMS to permutations of avalanche mass (fracture height and density). For every avalanche path 12 different fracture heights, released densities, erosion heights and eroded densities are permuted, keeping the LWC and snow temperature constant. Markers and colors as in Fig. 5.

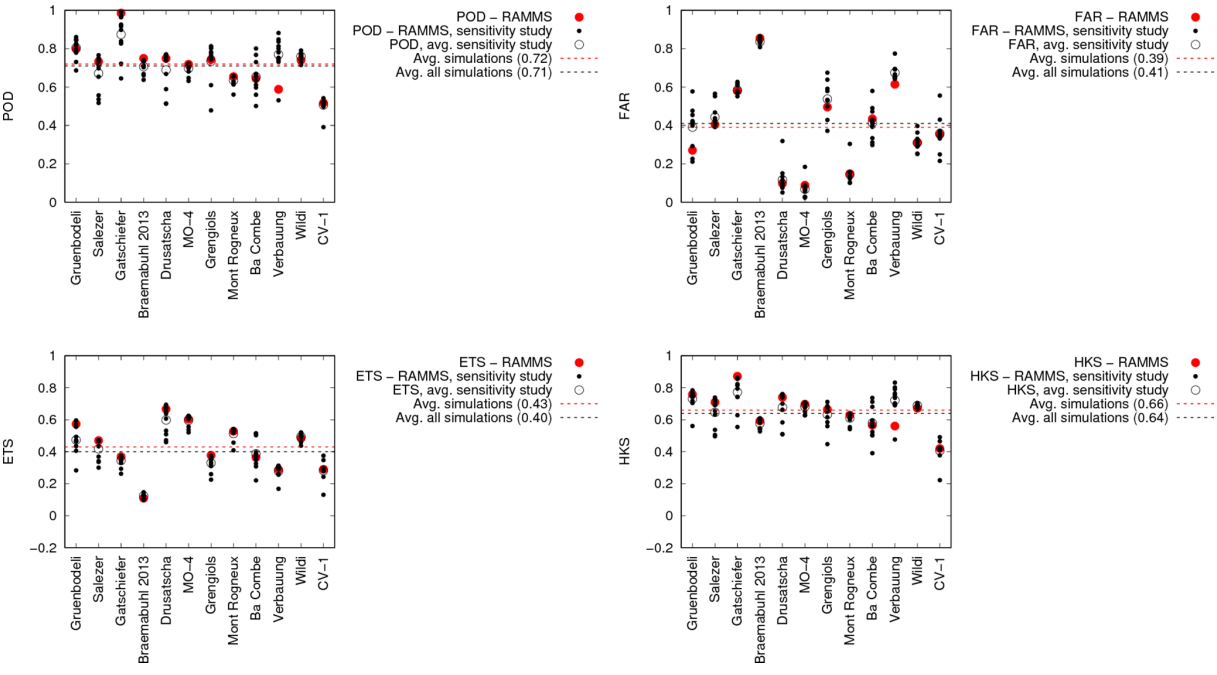

Figure 7. Sensitivity of the thermomechanical model to different snow temperature and LWC. For every avalanche path 12 different snow temperatures and LWCs in the release and erosion zones are varied, keeping the release and eroded height and density constant. Markers and colors as in Fig. 5.

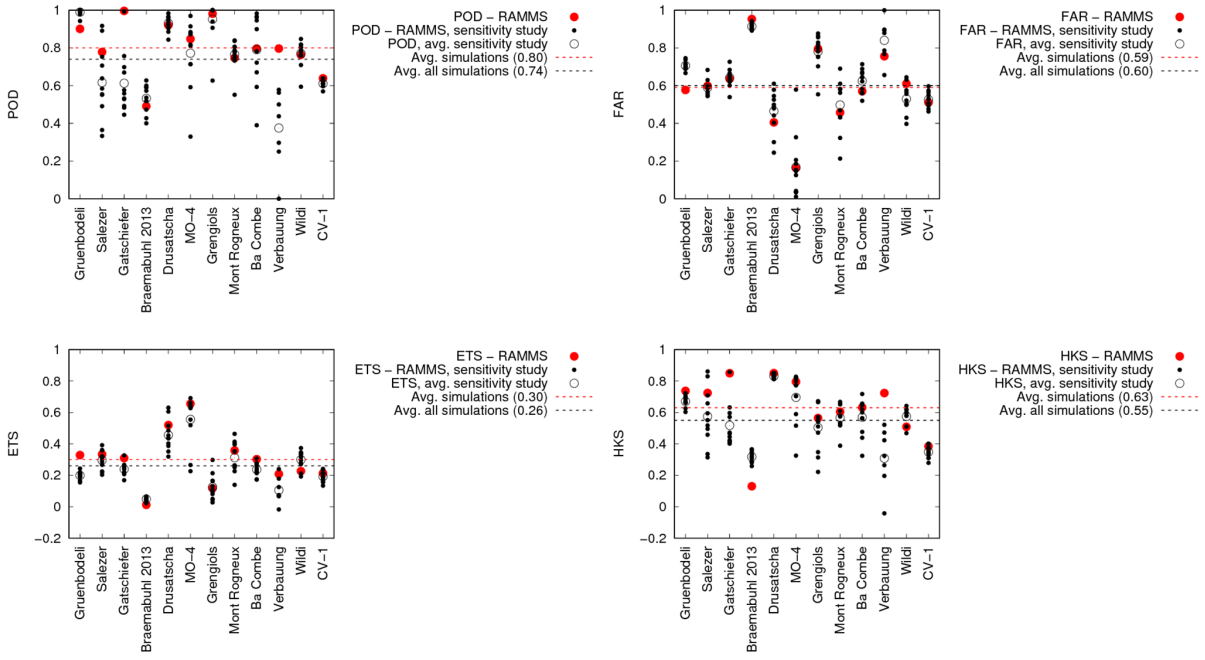

Figure 8. Sensitivity study simulating every avalanche path with the 12 different initial and boundary conditions, but with a simulation resolution (grid size) of 10 m for the 144 simulations (compare to Fig. 5 for 3 m resolution). Markers and colors as in Fig. 5.

for the 5 m resolution than for the 3 m resolution. However both obtained the same score in the HKS indicator. The results obtained in the ETS and HKS indicators show the same tendency observed in the comparison between 3 and 10 m. Coarser resolutions lead not only to overflowing and obtaining more hits but also to more false alarms, which penalize the overall score. Nevertheless, in the case of 3 and 5 m, it is necessary to compare avalanche path by avalanche path and to check which resolution better suits a particular avalanche path. Narrow, steep gullies with pronounced topographic features (Ba Combe, MO-4 and CV-1) require higher resolution than open slopes (Drusatscha, Mont Rogneux, Wildi and Gatschiefer).

In summary, we found the following results regarding grid resolution:

1. Changes in grid resolution lead to variations in statistical scores comparable to changes in initial conditions (mass and snow conditions).

2. There appears to be an optimal grid resolution between 3 and 5 m. Coarser resolutions (10 m) smooth out the terrain too much and lead to larger inundation areas and longer runouts.

3. For frequent avalanches (10-year return period) the 3–5 m resolution is adequate, based on the statistical scores. This implies that the digital smoothing is comparable to the natural smoothing of the snow cover over bare ground.

4. The 3 m resolution gives better statistical scores for avalanches following narrow gullies; the 5 m resolution gives better statistical scores for avalanches on open slopes.

4.4 Runout analysis study

A commonly used measure for avalanche size is the runout distance. Figure 10 shows the difference in simulated and measured runout distance for each studied avalanche for different grid cell sizes using the thermomechanical model RAMMS as well as the guideline-VS model. The absolute error in runout distance calculated by the thermomechanical model is about 3 times smaller than that predicted by the guideline-VS model. The difference between both models was larger on paths where the transition to the deposition zone was smoother (Drusatscha, Braemabuhl, Mont Rogneux, Ba Combe, Gatschiefer). On the paths where this transition is more pronounced, the calculated runout distances are closer (e.g., Gruenbodeli, MO-4, CV-1; see Fig. 10).

The analysis was repeated using two coarser grid resolutions (10 and 5 m cell size) for the thermomechanical model (see Fig. 10). In the case of 10 m resolution, the model tends to overrun measured runout distances. The average error between simulated and measured runout increases from around 49 with 3 m resolution to 72 with 10 m resolution. The difference between 3 and 5 m resolution is much smaller, and the 5 m resolution calculations slightly outperform the 3 m ones

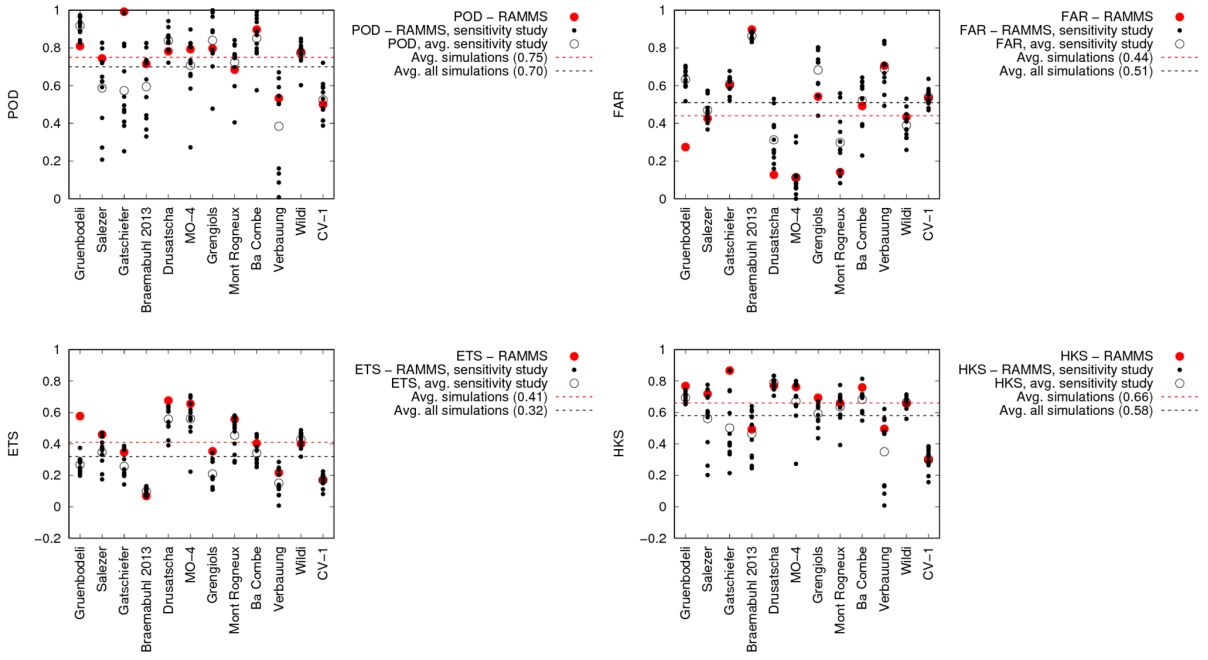

Figure 9. Sensitivity study simulating every avalanche path with the 12 different initial and boundary conditions, but with a simulation resolution (grid size) of 5 m for the 144 simulations (compare to Fig. 5 for 3 m resolution). Markers and colors as in Fig. 5.

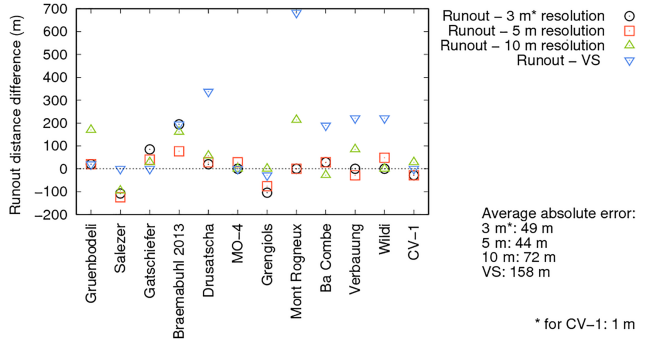

Figure 10. Runout error plot comparing thermomechanical wet-snow model calculations (black dots) with guideline-VS runout calculations (blue triangles), as well as runout calculations with 5 and 10 m model resolution with the thermomechanical model (red squares and green triangles, respectively). The legend shows the absolute average simulation error for each set of simulations. It was necessary to simulate the CV-1 case with a 1 m grid resolution to better account for a vertical wall.

in terms of runout distance. On the other hand, the 3 m resolution simulations show on average a higher ETS score than and equal HKS score to the 5 m simulations (see Sect. 4.3).

We repeated the sensitivity study for runout distance with three sets of 144 simulations interchanging the initial and boundary conditions as described in the previous section (see Fig. 11). The results obtained performing the sensitivity analysis confirmed the results achieved in the previous contingency analysis. The thermomechanical model is sensitive to changes in the initial and boundary conditions. Those changes are more important on avalanche paths where the transition to the runout is smooth. On those paths, changes in the initial and boundary conditions lead to deviations of hundreds of meters in runout calculations)Gatschiefer, Drusatscha, Mont Rogneux, Ba Combe; Fig. 11). The runout calculations were more sensitive to changes in mass than to changes in snow cover conditions (temperature and LWC). Varying the mass in the release and erosion doubles the absolute error obtained by varying only snow temperature and LWC.

5 Discussion

Our analysis is limited to evaluating deposition areas and runout distances for the 12 case studies. Other important avalanche variables – such as speed, dynamic flow heights and impact pressures – are not considered in the analysis, although they are crucial in many aspects of assessing avalanche risks. Thus, we are considering only one primary component of the avalanche flow problem: calculating the area covered by the avalanche deposits. We circumvent the lack of flow data by considering well-documented avalanche case studies in a single flow regime (wet) with return periods of approximately 10 to 30 years. An advantage of this approach is that we consider more than one track geometry, allowing us to draw conclusions about the application of

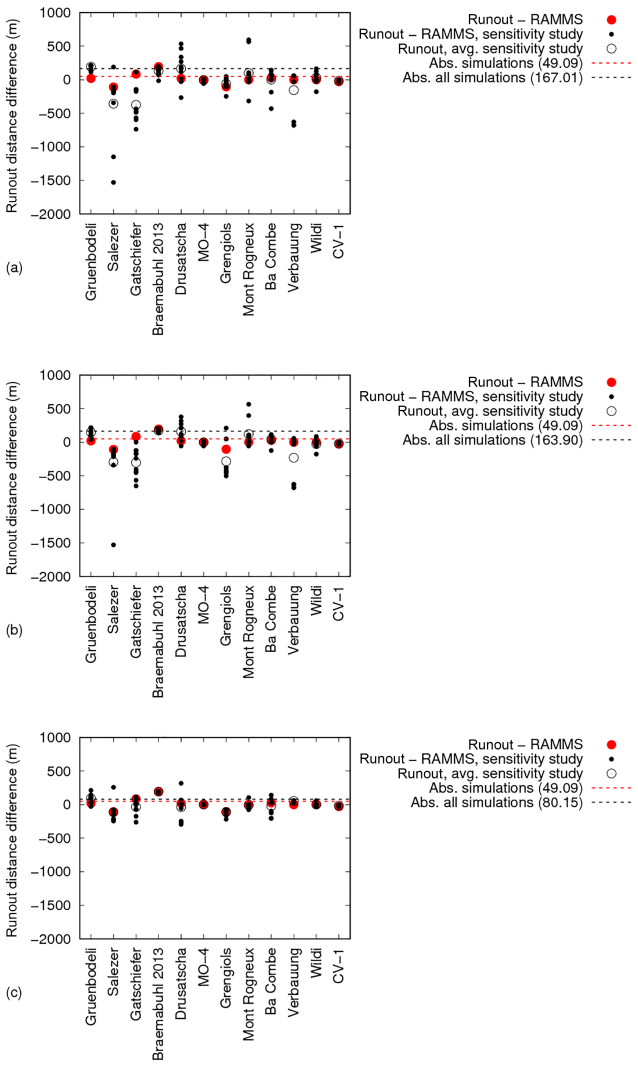

Figure 11. Difference between simulated and measured runout distance for the wet-snow model simulations with the corresponding initial conditions (red dots) and permutations (black dots). The average of the 11 permutations is depicted as a black open circle. **(a)** Varying both snow mass (fracture height and density) and snow properties (temperature and LWC), **(b)** varying snow mass only and **(c)** varying snow properties only. The red and black lines show the average absolute error in meters of the whole set of simulations (sensitivity and real simulations) to the runout distance measured in the field.

snow cover models and avalanche dynamics calculations in different terrain.

The starting mass was specified by performing snow cover simulations to determine the fracture height, density, temperature and water content of the release zone. The snow cover simulations were driven by measured meteorological data from stations near the release zone. The spatial extent of the release was known from observations and/or measurements. Having accurate information on where the avalanche released contributes significantly to the goodness of the statistical scores. Knowing the location of the release zone and a DEM of the avalanche track predetermines the flow path of the avalanche in the simulations, making a contingency table analysis useful. The model has one parameter α (Buser and Bartelt, 2009), which depends on the avalanche path and still has to be chosen by the avalanche expert. Therefore the application will demand experience in terrain and modeling of avalanches by the avalanche expert, even though the range of α is well constrained (Vera Valero et al., 2016).

An advantage of the contingency table analysis is that it can be used to identify tracks where there will be a large variability in runout depending on the initial conditions. Our analysis of the simulations revealed a large variability in predicted runout for tracks with flat terraces and gradual slope transitions to the runout zone. Here, we showed that the results are very sensitive to the specification of mass in the release and entrainment zones. On these tracks, an underestimation of fracture height of only 10 cm could lead to significant runout shortening and underestimation of the affected area. However, the initial and boundary conditions estimated from snow cover modeling have demonstrated a good accuracy in the overall results; the red dots on Figs. 5, 6 and 7 show on average better statistical scores than the black dots calculated with the variations. This result suggests statistically that initial conditions derived from snow cover modeling improve randomly chosen initial conditions derived from a set of wet-snow avalanche days. Once again, although the coupling between the snow cover modeling and avalanche dynamics calculations can be automatized, the sensitivity analysis suggests that a mistake in the mass estimation can lead to entirely wrong results. We emphasize that we come to this conclusion even though we have restricted our attention to a single avalanche flow regime. Nonetheless, the coupling of snow cover models and avalanche simulations could provide avalanche services with more information to make a risk assessment. Using avalanche dynamics models in this way differs from traditional avalanche calculations, which are based on extreme conditions, with no link to particular snow cover or meteorological conditions.

The general thermomechanical avalanche dynamics model RAMMS performs better than the guideline-VS model in all statistical scores: HKS, ETS, POD and FAR (see Fig. 4). The guideline procedures are designed to model extreme dry-flowing avalanches, not particular avalanche events. However, the guideline model achieved in some cases high contingency table scores, despite the application on non-extreme wet-snow avalanches. The guideline-VS model was forced using friction coefficients calibrated by Salm et al. (1990). It was necessary to use the friction coefficients corresponding to smaller avalanche sizes in order to achieve a good correspondence between measurements and simulations. For all case studies, the friction coefficients chosen correspond to size class “small” and a return period of 10 to 30 years. The guideline-VS model had to be manipulated by an expert

user to get the best results. For example, the general model was first applied to determine the mass balance of the event, which was then used to establish the initial conditions (i.e., released plus eroded mass) of the guideline-VS model. Another disadvantage of the guideline model is that first a calibration of the friction parameters is required to obtain reasonable contingency table scores. Both steps are not required in the general model applications, because the friction parameters are determined as a known function of snow cover conditions.

Because we considered only wet-snow avalanches, the range of snow temperature was rather narrow and close to zero. The water content varied between 1 and 5 %, which is a typical range of bulk LWC for slopes (Heilig et al., 2015). The vertical liquid water distribution typically exhibited a thin layer with high LWC located near layer boundaries (capillary barriers), which supports the assumption in the avalanche model that the liquid water is concentrated at the sliding surface. The results of the snow cover simulations were visually inspected to determine the avalanche fracture height (following Wever et al., 2016). This height could be verified by the observations of the actual release zone. The bulk LWC of the slab above the depth of the maximum local LWC was used to initialize the simulations. In general, the statistical scores of the contingency table analysis did not change much as a function of the water content. However, changing water content in some cases led to a large difference in simulated inundation area and runout distance. These cases are associated with terrain characteristics and their influence on the rate of meltwater production as well as the LWC of the eroded snow. For example, the Grengiols and Mont Rogneux avalanche case studies stopped on a flat zone when the initial liquid water was reduced below the simulated SNOWPACK value. This indicates that underestimated LWC can lead to spurious runout shortening. In general, however, variations of mass (i.e., fracture and erosion heights together with snow density) produced larger variations in the final simulation results (see Fig. 5, 6 and 7). The mass variations in the sensitivity analysis were broad; see Table 1. Therefore, when using this set of case studies with only wet-snow avalanche cases, the model is more sensitive to changes in avalanche mass than in snow cover conditions (LWC and snow temperature).

The statistical scores of the contingency table analysis are dependent on the grid resolution of the avalanche dynamics calculations. The 10 m resolution appears to be far too coarse for the avalanche sizes of the case study examples. The contingency scores of the 3 and 5 m resolutions are similar. However, the 3 m runout calculations show a trend towards slightly shorter runout distances. The statistical scores of the 3 m resolution are overall better than the 5 m resolution because the 3 m scores were not penalized by excess runout and therefore obtained fewer false alarms. The 5 m resolution clearly achieved the best results for open slopes with gradual transition zones. A 3 m resolution might still be necessary when the track contains narrow gullies, bare ground or shallow snow covers where terrain features, including the presence of blocky scree, can play an important role. Deposition patterns of the smaller events can clearly be better represented by the finer 3 m resolution.

6 Conclusions

We used the physics-based snow cover model SNOWPACK to set the initial conditions for avalanche dynamics calculations. We restricted our attention to avalanches in one flow regime (wet) where the height and spatial extent of the avalanche release area was known. We used a contingency table analysis to statistically evaluate how well avalanche dynamics models can predict deposition area and runout distances. Although we can demonstrate that physics-based models improve the statistical scores, we note that in certain track geometries the results of the avalanche dynamics calculations are extremely sensitive to the specification of the correct starting conditions, particularly fracture and entrainment heights. These tracks contain flat track segments below the release zone and gradual transition zones leading towards the avalanche runout zone. In these cases, underestimating fracture heights and entrainment heights can lead to significant underprediction of avalanche runout distances. The problem appears not to be with the quality of the avalanche dynamics simulations, but it illustrates that for these cases it is crucial that numerical snow cover models accurately predict the state of the snowpack from data measured from automatic weather stations.

The model chain could be applied in regions where considerable experience and knowledge of local snow cover variability and avalanche history exist. As these conditions change from year to year, a complete cadaster of documented events is still invaluable. There are cases where these conditions are fulfilled; see Vera Valero et al. (2016). In these situations the model chain can support decisions on a deterministic basis and provide decision makers with a valuable source of information about current avalanche risks.

Data availability. Data are available on request.

The Supplement related to this article is available online at https://doi.org/10.5194/nhess-18-869-2018-supplement.

Competing interests. The authors declare that they have no conflict of interest.

Acknowledgements. Financial support for this project was provided by Codelco Mining, Andina Division (Chile). We thank all Codelco

avalanche alert center members – Luis Gallardo, Marcel Didier and Patricio Cerda – together with the Mountain Safety crew, not only for their support but also for their confidence, patience and enormous help during the last four winters in the Andina mine.

Edited by: Sven Fuchs
Reviewed by: Jan-Thomas Fischer and Guillaume Chambon

References

Bartelt, P. and Buser, O.: Avalanche dynamics by Newton. Reply to comments on avalanche flow models based on the concept of random kinetic energy, J. Glaciol., 64, 165–170, https://doi.org/10.1017/jog.2018.1, 2018.

Bartelt, P. and Lehning, M.: A physical SNOWPACK model for the Swiss avalanche warning Part I: Numerical model, Cold Reg. Sci. Technol., 35, 123–145, https://doi.org/10.1016/S0165-232X(02)00074-5, 2002.

Bartelt, P. and McArdell, B.: Granulometric investigations of snow avalanches, J. Glaciol., 55, 829–833, 2009.

Bartelt P., Buser, O., and Martin K.:Dissipated work, stability and the internal flow structure of granular snow avalanches, J. Glaciol., 51, 125–138, 2005.

Bartelt P., Buser, O., and Platzer K.:Fluctuation-dissipation relations for granular snow avalanches, J. Glaciol., 52, 631–643, 2006.

Bartelt, P., Bühler, Y., Buser, O., Christen, M., and Meier, L.: Modeling mass-dependent flow regime transitions to predict the stopping and depositional behaviour of snow avalanches, J. Geophys. Res., 117, F01015, https://doi.org/10.1029/2010JF001957, 2012a.

Bartelt, P., Glover, J., Feistl, T., Bühler, Y., and Buser, O.: Formation of levees and en-echelon shear planes during snow avalanche runout, J. Glaciol., 58, 980–992, https://doi.org/10.3189/2012JoG11J011, 2012b.

Bartelt, P., Vera Valero, C., Feistl, T., Christen, M., Bühler, Y., and Buser, O.: Modelling Cohesion in Snow Avalanche Flow, J. Glaciol., 61, 837–850, https://doi.org/10.3189/2015JoG14J126, 2015.

Bozhinskiy, A. N. and Losev, K. S.: The fundamentals of avalanche science, Mitt. Eidgenöss. Inst. Schnee- Lawinenforsch., Davos, 280 pp., 1998.

Bühler, Y., Christen, M., Kowalsky, J., and Bartelt, P.: Sensitivity of snow avalanche simulations to digital elevation model quality and resolution, Ann. Glaciol., 52, 72–80, 2011.

Buser, O. and Bartelt, P.: Production and decay of random kinetic energy in granular snow avalanches, J. Glaciol., 55, 3–12, 2009.

Buser, O. and Bartelt, P.: An energy-based method to calculate streamwise density variations in snow avalanches, J. Glaciol., 61, 563–575, https://doi.org/10.3189/2015JoG14J054, 2015.

Christen, M., Kowalski, J., and Bartelt, P.: RAMMS: Numerical simulation of dense snow avalanches in three-dimensional terrain, Cold Reg. Sci. Technol., 63, 1–14, https://doi.org/10.1016/j.coldregions.2010.04.005, 2010.

Colbeck, S.: A review of the processes that control snow friction, Cold Regions Research and Engineering Lab, 92–2, 40 pp., 1992.

Dent, J. D. and Lang, T. E.: A biviscous modified Bingham model of snow avalanche motion, Ann. Glaciol., 4, 42–46, 1983.

Dent, J. D., Burrell, K., J., Schmidt, D. S., Louge, M. Y., Adams, E. E., and Jazbutis, T. G.: Density, velocity and friction measurements in a dry snow avalanche, Ann. Glaciol., 26, 247–252, 1998.

Denoth, A.: The Pendular-Funicular Liquid Transition and Snow Metamorphism. J. Glaciol., 28, 357–364, 1982.

Fischer, J., Kowalski, J., and Pudasaini, S.: Topographic curvature effects in applied avalanche modeling, Cold Reg. Sci. Technol., 74–75, 21–30, https://doi.org/10.1016/j.coldregions.2012.01.005, 2012.

Glenne, B.: Sliding friction and boundary lubrication of snow, J. Tribol., 109, 614–617, 1987.

Gruber, U. and Bartelt, P.: Snow avalanche hazard modeling of large areas using shallow water numerical methods and GIS, Environ. Modell. Softw., 22, 1472–148, 2007.

Gubler, H.: Measurements and modelling of snow avalanche speeds, International Association of Hydrological Sciences Publication 162, Symposium at Davos 1986 – Avalanche Formation, Movement and Effects, 405–420, 1987.

Heilig, A., Mitterer, C., Schmid, L., Wever, N., Schweizer, J., Marshall, H., and Eisen, O.: Seasonal and diurnal cycles of liquid water in snow – Measurements and modeling, J. Geophys. Res.-Earth, 120, 2139–2154, https://doi.org/10.1002/2015JF003593, 2015.

Jomelli, V. and Bertran, P.: Wet snow avalanche deposits in the French Alps: structure and sedimentology, Geogr. Ann. A, 83, 15–28, 2001.

Kern, M., Bartelt, P., Sovilla, B., and Buser, O.: Measured shear rates in large dry and wet snow avalanches, J. Glaciol., 55, 327–338, 2009.

Lehning, M. and Fierz, C.: Assessment of snow transport in avalanche terrain, Cold Reg. Sci. Technol., 51, 240–252, 2008.

Lehning, M., Bartelt, P., Brown, B., Fierz, C., and Satyawali, P.: A physical SNOWPACK model for the Swiss avalanche warning Part II: Snow microstructure, Cold Reg. Sci. Technol., 35, 147–167, https://doi.org/10.1016/S0165-232X(02)00073-3, 2002.

Naaim, M., Durand, Y., Eckert, N., and Chambon, G.: Dense avalanche friction coefficients: influence of physical properties of snow, J. Glaciol., 59, 771–782, 2013.

Norem, H., Irgens, F., and Schieldrop, B.: A continuum model for calculating snow avalanche velocities, International Association of Hydrological Sciences Publication, 162, Symposium at Davos 1986 – Avalanche Formation, Movement and Effects, 363–379, 1987.

Platzer, K., Bartelt, P., and Kern, M.: Measurements of dense snow avalanche basal shear to normal stress ratios (S / N), Geophys. Res. Lett., 34, L07501, https://doi.org/10.1029/2006GL028670, 2007.

Salm, B.: Mechanical propoerties of snow, Reviews of Geophysics and Space Physics, 20, 1–19, 1982.

Salm, B.: Flow, flow transition and runout distances of flowing avalanches, Ann. Glaciol., 18, 221–226, 1993.

Salm, B., Burkard, A., and Gubler, H.: Berechnung von Fliesslawinen: eine Anleitung fuer Praktiker mit Beispielen, Eidg. Inst. Schnee- und Lawinenforschung Mitteilung, 47, 1–37, 1990.

Vera Valero, C., Bühler, Y., Wikstroem Jones, K., and Bartelt, P.: Release Temperature, Snowcover Entrainment and the Thermal Flow Regime of Snow Avalanches, J. Glaciol., 61, 173–184, 2015.

Vera Valero, C., Wever, N., Bühler, Y., Stoffel, L., Margreth, S., and Bartelt, P.: Modelling wet snow avalanche runout to assess road safety at a high-altitude mine in the central Andes, Nat. Hazards Earth Syst. Sci., 16, 2303–2323, https://doi.org/10.5194/nhess-16-2303-2016, 2016.

Voellmy, A.: Ueber die Zerstoerungskraft von Lawinen, Schweiz. Bauztg., 73(19), 280–285, (12), 159–162, (15), 212–217, (17), 246–249, (19), 280–285, 1955.

Voytkovskiy, K. F.: Mekhanicheskiye svoystva snega, [Mechanical properties of snow)], Moscow, Nauka, Sibirskoye Otdeleniye, Institut Merzlotovedeniya, translated by: Bartelt, C. E., 1977.

Wever, N., Fierz, C., Mitterer, C., Hirashima, H., and Lehning, M.: Solving Richards Equation for snow improves snowpack meltwater runoff estimations in detailed multi-layer snowpack model, The Cryosphere, 8, 257–274, https://doi.org/10.5194/tc-8-257-2014, 2014.

Wever, N., Schmid, L., Heilig, A., Eisen, O., Fierz, C., and Lehning, M.: Verification of the multi-layer SNOWPACK model with different water transport schemes, The Cryosphere, 9, 2271–2293, https://doi.org/10.5194/tc-9-2271-2015, 2015.

Wever, N., Vera Valero, C., and Fierz, C.: Assessing wet snow avalanche activity using detailed physics based snowpack simulations, Geophys. Res. Lett., 43, 5732–5740, 2016.

Woodcock, F.: The Evaluation of Yes/No Forecasts for Scientific and Administrative Purposes, Mon. Weather Rev., 104, 1209–1214, 1976.